

# Coupling and Electrical Control of Structural, Orbital and Magnetic Orders in Perovskites

Julien Varignon,<sup>†,‡</sup> Nicholas C. Bristowe,<sup>†,‡</sup> Eric Bousquet,<sup>†</sup> and Philippe  
Ghosez<sup>\*,†</sup>

*Physique Théorique des Matériaux, Université de Liège (B5), B-4000 Liège, Belgium*

E-mail: philippe.ghosez@ulg.ac.be

## Abstract

Perovskite oxides are already widely used in industry and have huge potential for novel device applications thanks to the rich physical behaviour displayed in these materials. The key to the functional electronic properties exhibited by perovskites is often the so-called Jahn-Teller distortion. For applications, an electrical control of the Jahn-Teller distortions, which is so far out of reach, would therefore be highly desirable. Based on universal symmetry arguments, we determine new lattice mode couplings that can provide exactly this paradigm, and exemplify the effect from first-principles calculations. The proposed mechanism is completely general, however for illustrative purposes, we demonstrate the concept on vanadium based perovskites where we reveal an unprecedented orbital ordering and Jahn-Teller induced ferroelectricity. Thanks to the intimate coupling between Jahn-Teller distortions and electronic degrees of freedom, the electric field control of Jahn-Teller distortions is of general relevance and may find broad interest in various functional devices.

---

\*To whom correspondence should be addressed

<sup>†</sup>Physique Théorique des Matériaux, Université de Liège (B5), B-4000 Liège, Belgium

<sup>‡</sup>These two authors contributed equally

# Introduction

Widespread interest in transition metal perovskite-like oxides over the last several decades can be ascribed to two key discoveries: high-temperature superconductivity in the cuprates and colossal magnetoresistance in the manganites.<sup>1-4</sup> Physical behavior exhibited by perovskites is by no means limited to these two phenomena, including ferroelectricity (e.g. titanates) and (anti)ferromagnetism or both simultaneously and coupled in magnetoelectric multiferroics (e.g. ferrites, manganites), metal-insulator transitions (e.g. nickelates) and thermoelectricity (e.g. cobaltites), to name a few. The wide range of functional properties is usually thanks to an interplay between the structural (lattice), electronic (orbital and charge) and magnetic (spin) degrees of freedom allowed within the transition metal oxides.<sup>5-8</sup> This playground for novel materials physics is not only of fundamental academic interest, but oxide perovskites have already entered industry and have huge potential for novel device applications.<sup>9-11</sup>

The possibility of tuning the magnetic properties of a material with an applied electric field has received particular attention for low energy consumption spintronic devices.<sup>9,12</sup> In this regard, a promising route to achieve ferroelectricity in magnets is the so-called rotationally driven ferroelectricity.<sup>5-7</sup> Here one or more antiferrodistortive (AFD) motions, which are ubiquitous in perovskites, simultaneously drives the polarization and can couple to the magnetic orders.<sup>16-18</sup> However, the AFD motions are rather weakly linked to the electronic properties and hence the magnetoelectric coupling is likely not the most efficient. It would be advantageous to replace the AFD motions by another lattice distortion which couples directly to the electronic properties. Such a motion common in perovskites is the Jahn-Teller distortion, however there currently does not exist a clear and universal recipe to control Jahn-Teller distortion with an external electric field.

In the present work, we provide a pathway to achieve an electric field control of Jahn-Teller distortions in perovskites through universal symmetry arguments. Since Jahn-Teller distortions are intimately connected to electronic degrees of freedom,<sup>19</sup> such as magnetism, orbital orderings and metal-insulator phase transitions to name a few, the proposed mechanism may find broader interest for novel functional devices outside the field of magnetoelectrics. This mechanism is completely

general, however for illustrative purposes, we demonstrate the concept on the vanadate perovskites which exhibit a complex structural ground state including different Jahn-Teller distortions. The effect is further quantified through first-principles calculation. In  $AA'V_2O_6$  superlattices, we reveal an unprecedented orbital ordering and Jahn-Teller induced ferroelectricity and demonstrate an electric field control of the magnetization.

## **Bulk $A^{3+}V^{3+}O_3$**

Whilst the  $V^{4+}$  perovskites (e.g.  $SrVO_3$ ) have been studied mainly for their interesting metallic properties,<sup>20</sup> the  $V^{3+}$  perovskites are Mott insulators.  $A^{3+}V^{3+}O_3$  compounds have attracted much attention since the fifties when they were first synthesized.<sup>21</sup> During this time, many studies began to determine their magnetic, electronic and structural properties.<sup>1,4,22–25,27–32,34–39</sup> A central theme at the core of these properties in vanadates is the so-called Jahn-Teller (JT) distortion. The famous Jahn-Teller theorem claims that a material with degenerate electronic states will be unstable towards undergoing a structural distortion lowering its symmetry to remove the electronic degeneracy.<sup>40</sup> In other words, the JT effect is an electronic instability that can cause a structural and metal-insulator phase transition. For instance, in the cubic perovskite symmetry, the crystal field effect splits the  $d$  electron levels into a lower lying degenerate three-fold  $t_{2g}$  and a higher lying degenerate two-fold  $e_g$  state. Hence in  $3d^2$  systems such as the rare-earth vanadates, a Jahn-Teller distortion is required to split the  $t_{2g}$  levels in order to form a Mott insulating state.<sup>41</sup>

In the vanadates, two different Jahn-Teller distortions are observed.<sup>4,24,25,35</sup> The corresponding distortions are displayed in 1 where they are compared to the so-called antiferrodistortive (AFD) motions that appear abundantly in perovskites. The AFD motions can be viewed as oxygen octahedra rotations around an axis going through the B cations, while the JT distortions correspond to oxygen rotations around an axis going through the A cations. Both JT and AFD motions can be either in-phase (1.a+b) or anti-phase (1.c+d) between consecutive layers and therefore appear at the M or R points of the Brillouin zone respectively. Consequently, we label the Jahn-Teller dis-

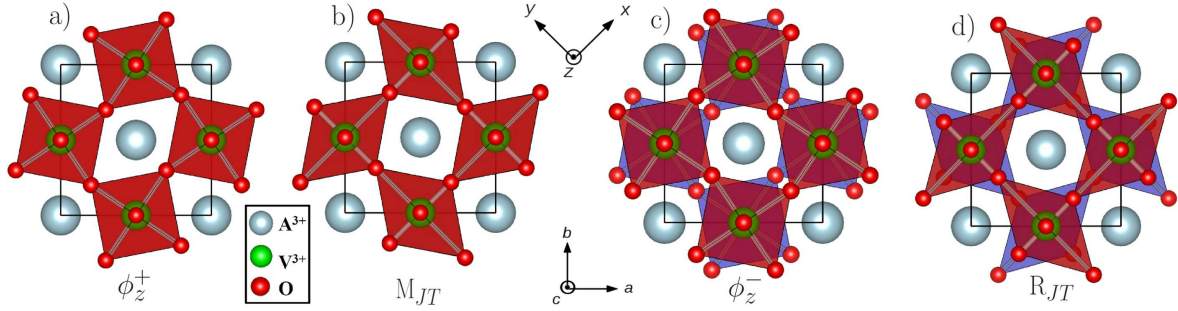


Figure 1: Comparison of JT and AFD motions around the  $z$  axis; a) in-phase  $\Phi_z^+$  AFD motion; b) in-phase  $M_{JT}$  Jahn-Teller motion; c) anti-phase  $\Phi_z^-$  motion; d) anti-phase  $R_{JT}$  motion. Octahedra for the plane in  $z=0$  are plotted in red and in blue for the plane in  $z=c/2$ . The AFD motions can also appear around the  $y$  and  $z$  axes (not shown), whereas the Jahn-Teller motions only manifest around the  $z$  axis in the vanadates.

tortions as  $M_{JT}$  and  $R_{JT}$ . While AFD motions do not distort the  $BO_6$  octahedra and appear purely through steric effects, JT motions lift the degeneracy of the  $d$  levels through octahedra deformations. According to such distortions, the  $V^{3+} 3d^2$  occupation consists of either a  $d_{xy}$  and  $d_{xz} t_{2g}$  or a  $d_{xy}$  and  $d_{yz} t_{2g}$  state. Nearest-neighbor vanadium sites within the  $(xy)$ -plane develop opposite distortions and hence alternative  $d_{xy}$  and  $d_{xz} / d_{xy}$  and  $d_{yz}$  occupations as shown in the top panel of 2. Along the  $c$  axis, the octahedra deformations and hence orbital ordering are either in phase (C-type orbital order) or anti-phase (G-type orbital order) for the M or R Jahn-Teller distortion respectively (see 2 middle panel). Crucially, the orbital ordering determines the magnetic ordering through superexchange interactions.<sup>42–46</sup> Strongly overlapping and parallel orbitals between neighboring sites favors antiferromagnetic superexchange interactions. With this in mind, the  $M_{JT}$  favors a purely antiferromagnetic solution called AFMG whilst the  $R_{JT}$  favors  $(xy)$ -plane antiferromagnetic alignment and ferromagnetic out-of-plane alignment called AFMC (see 2 bottom panel). Experiments indeed observe both AFMG and AFMC magnetic phases in the vanadates, with each magnetic ordering favoring a certain structural symmetry.<sup>4,25,35</sup>

At room temperature, all rare-earth  $A^{3+}V^{3+}O_3$  vanadates crystallize in a  $Pbnm$  structure. With decreasing temperature, the vanadates undergo an orbital ordering phase transition to a G-type orbital ordered (G-o.o.) phase between 200K and 150K (depending on the A-cation size). This

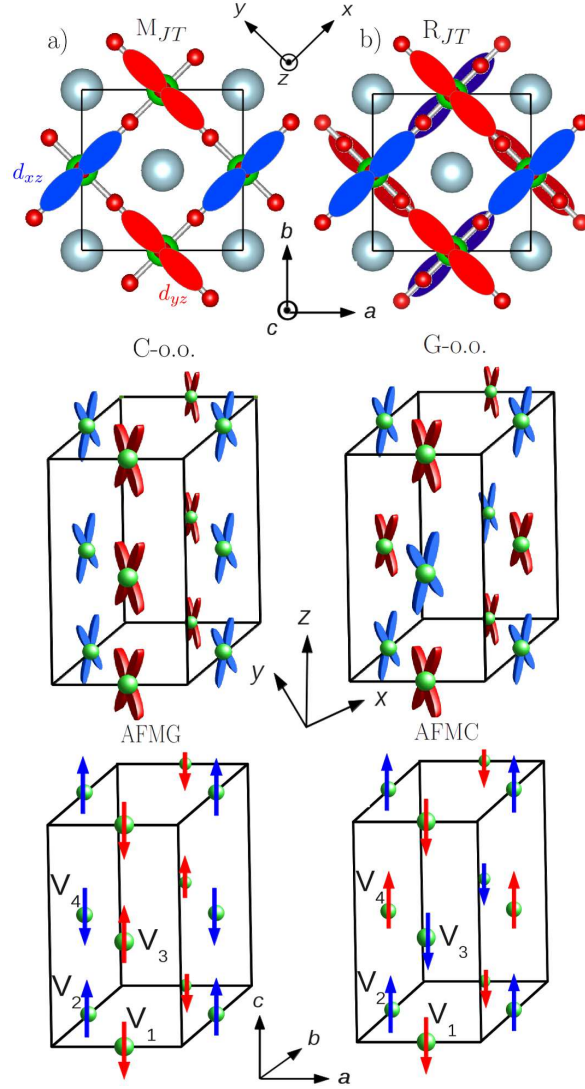


Figure 2: Schematic picture of the idealized orbital orderings between the  $d_{xz}$  (blue) and  $d_{yz}$  (red) orbitals. The  $d_{xy}$  orbital is not shown for clarity. a) Top view of the orbital-ordering induced by a  $M_{JT}$  distortion (top). Consecutive planes exhibit identical orbital orderings labelled as a C-type orbital-ordering (C-o.o.) (middle). This results in a AFMG ordering (bottom). b) Orbital-ordering induced by a  $R_{JT}$  distortion (top). Consecutive planes exhibit out-of phase orbital orderings labelled as a G-type orbital-ordering (G-o.o.) (middle). This results in a AFMC ordering (bottom).

transition is accompanied by a symmetry lowering from  $Pbnm$  to  $P2_1/b$ . A magnetic phase transition from a paramagnetic to an AFMC antiferromagnetic state occurs within this phase at a slightly lower temperature between 150K and 100K. Finally, for the smallest A cations (A=Yb-Dy, Y), another orbital ordering phase transition to a purely C-type (C-o.o.) arises and is accompanied by a structural phase transition from  $P2_1/b$  back to  $Pbnm$ , and a magnetic phase transition from AFMC to AFMG. For medium A cations (A=Tb-Nd), a coexisting orbital-ordering state (C+G-o.o.) is found with no structural symmetry change. No further transitions are found for larger A cations (A=Pr, Ce and La), which remain in the AFMC G-o.o.  $P2_1/b$  phase.

It is interesting to note a couple observations. Firstly both the G-o.o. and AFMC magnetic ordering phases are very rare amongst oxide perovskites. Secondly the coexisting orbital-orderings appearing for medium A-size cations is curious, and there is some debate whether this mixed state is phase separated or coexisting within the same phase.<sup>4,25</sup> To attempt to shed light on some of these issues, we perform a symmetry mode analysis of the allowed distortions with respect to a hypothetical cubic phase on three different,<sup>47,48</sup> but typical, vanadates:  $YVO_3$ ,  $PrVO_3$  and  $LaVO_3$ .  $YVO_3$  is known to present a  $Pbnm$  ground state with a C-o.o. (AFMG) at low temperature, and a  $P2_1/b$  state with a G-o.o. (AFMC) at higher temperatures, while  $LaVO_3$  and  $PrVO_3$  only develop a  $P2_1/b$  ground state with a G-o.o. character (AFMC). The analysis is performed on experimental structural data, and the amplitudes of distortions are summarized in 1. The experimental structural data are well represented in our first principles calculations (see supplementary material).<sup>2,4,23,38,50</sup>

In the  $Pbnm$  phase ( $a^-a^-c^+$  in Glazer's notations),<sup>51</sup> all vanadates develop two unique AFD motions  $\phi_{xy}^-$  ( $\phi_{xy}^- = \phi_x^- + \phi_y^-$ ) and  $\phi_z^+$ . Table 1 shows that the magnitudes of these AFD motions strengthen with decreasing A-cation size as expected via simple steric arguments.<sup>52</sup> In this symmetry, the  $M_{JT}$  distortion is also allowed and amazingly, this distortion is already present at room temperature and for all A-cations. This finding is in contradiction with previous reports of a C-o.o. phase only for small A cations below 100K.<sup>4,25</sup> Our analysis based solely on experimental data suggests a C-o.o. should already exist at room temperature, and has likely been overlooked until now. The  $Pbnm$  phase then appears to always be a pure  $M_{JT}$  phase. Additionally, an anti-polar  $X_5^-$

Table 1: Amplitudes of distortions (in Å) on experimental structures of vanadates at different temperatures. In the  $P2_1/b$  symmetry, both  $\phi_{xy}^-$  and  $\phi_z^-$  AFD motions belong to the same irreducible representation. The reference structure was chosen as a cubic structure whose lattice vector corresponds to the pseudo cubic lattice vector associated to the room temperature  $Pbnm$  phase. One should notice that for the  $P2_1/b$  phase, both  $\phi_{xy}^-$  and  $\phi_z^-$  motions belong to the same irreps, even if the  $\phi_z^-$  amplitude should be extremely small.

Irreps	YVO <sub>3</sub>		PrVO <sub>3</sub>		LaVO <sub>3</sub>		
	$Pbnm$ 295K <sup>2</sup>	$P2_1/b$ 100K <sup>38</sup>	$Pbnm$ 5K <sup>2</sup>	$Pbnm$ 295K <sup>4</sup>	$P2_1/b$ 5K <sup>4</sup>	$Pbnm$ 298K <sup>50</sup>	$P2_1/b$ 10K <sup>23</sup>
$\phi_{xy}^- (+\phi_z^-)$	-	1.72	-	-	1.34	-	1.16
$\phi_{xy}^-$	1.71	-	1.73	1.34	-	1.17	-
$\phi_z^+$	1.22	1.24	1.22	0.94	0.96	0.68	0.75
$M_{JT}$	0.05	0.06	0.14	0.02	0.02	0.08	0.01
$R_{JT}$	-	0.10	-	-	0.18	-	0.08
$X_5^-$	0.86	0.87	0.87	0.53	0.64	0.37	0.39
$X_3^-$	-	0.01	-	-	0.06	-	0.00

mode whose motion is in the  $(xy)$ -plane is allowed in the  $Pbnm$  symmetry. Going to the  $P2_1/b$  symmetry, a subgroup of  $Pbnm$ , the aforementioned AFD motions are still present, but the  $R_{JT}$  distortion is now allowed and would lead to a G-o.o. phase. However, in contradiction to what was sometimes believed,<sup>4,25</sup> the  $P2_1/b$  phase is never an exclusive  $R_{JT}$  phase but always coexists with the  $M_{JT}$  distortion, even for the larger A cations (A=Pr, La). A mixed C+G-o.o. should then manifest for all  $P2_1/b$  structures. Additionally, another anti-polar  $X_3^-$  mode, whose motion is now along the  $z$  direction, arises in this new phase.

In order to understand the origin and coupling between these distortions, we can perform a free energy  $\mathcal{F}$  expansion (see methods) around a hypothetical cubic  $Pm\bar{3}m$  phase with respect to the different distortions. In the  $Pbnm$  phase, two trilinear couplings are involved in the free energy:

$$\mathcal{F}_{tri,Pbnm} \propto \phi_{xy}^- \phi_z^+ X_5^- + \phi_{xy}^- X_5^- M_{JT} \quad (1)$$

As already mentioned, the two robust AFD modes ( $\phi_{xy}^-$  and  $\phi_z^+$ ) are the primary lattice motions

producing the  $Pbnm$  symmetry. When  $\phi_{xy}^-$  and  $\phi_z^+$  are non zero in magnitude, the energy of the system is automatically lowered by the appearance of  $X_5^-$  due to the first trilinear term of Equation 1. Similarly, thanks to the second trilinear coupling, the energy of the system is lowered by the subsequent appearance of the  $M_{JT}$  distortion. This latter trilinear coupling explains why the  $M_{JT}$  is always present in the  $Pbnm$  phase of vanadates, even at room temperature. This demonstrates that, in addition to its possible appearance as an electronic instability, it will always appear as a structural anharmonic improper mode within the  $Pbnm$  phase (whose strength depends on the coupling constant) even in non magnetic materials. Going to the  $P2_1/b$  phase, two additional trilinear couplings are identified:

$$\begin{aligned} \mathcal{F}_{tri,P2_1/b} \propto & \phi_{xy}^- \phi_z^+ X_5^- + \phi_{xy}^- X_5^- M_{JT} \\ & + M_{JT} R_{JT} X_3^- + \phi_z^+ X_3^- \phi_z^- \end{aligned} \quad (2)$$

As previously mentioned, from experimental observations an orbital-ordering phase transition to a G-o.o. phase occurs between 150K and 200K for all vanadates,<sup>4,25</sup> which indicates that the  $R_{JT}$  is likely appearing as a primary electronic instability. Consequently, through the third trilinear coupling of Equation 2, both JT distortions produce the additional anti polar  $X_3^-$  motion, in agreement with the experimental data of 1. Finally, an extra  $\phi_z^-$  AFD motion arises in the  $P2_1/b$  phase, through the last trilinear coupling. The combination of in-phase and anti-phase rotations along the same axis,  $\phi_z^-$  and  $\phi_z^+$ , in the  $P2_1/b$  phase of the vanadates is a rare tilt-system ( $a^- a^- c^\pm$  in Glazer's notation), previously unknown in bulk perovskites to the best of the authors' knowledge.

Therefore, within this  $P2_1/b$  phase, both JT distortions coexist, but likely with different origins. The  $M_{JT}$  is "pinned" into the system through an improper anharmonic coupling with the robust AFD motions while the  $R_{JT}$  appears through the traditional Jahn-Teller electronic instability. It is interesting to note that this coexistence is allowed due to the improper appearance of  $M_{JT}$ , despite there likely being a competition between both JTs. This competition would be understood as an electronic origin to favor one type of orbital ordering over the other, producing a biquadratic



coupling with a positive coefficient in the free energy expansion. In the light of there being an abundance of  $M_{JT}$  with respect to  $R_{JT}$  phases across the perovskites, we then propose whether it is this improper appearance of  $M_{JT}$  via the robust AFD motions that helps favor this phase universally. The vanadates would then be a special case where the  $R_{JT}$  instability is robust enough to appear despite this competition. This universal symmetry analysis explains the origin of the coexisting orbital ordered phase in the  $Pb$  symmetry as observed in vanadates both experimentally and from first principles calculations.<sup>4,25,39</sup>

The coexistence of both JT motions in the vanadates, will also clearly affect the orbital and magnetic orderings. One might expect a complex canted magnetic ordering to occur, resembling partly AFMC and partly AFMG, as indicated experimentally from neutron scattering on several vanadates. Indeed, the observed non-collinear spin arrangement in the  $P2_1/b$  phase develops an AFMC ordering in the  $(xy)$ -plane and a weaker AFMG ordering along the  $c$  axis.<sup>2,29,30</sup> Interestingly, even at the collinear level, our first principles calculations already indicate this complex magnetic ordering in the  $P2_1/b$  phase. Within the  $YVO_3$   $Pbnm$  AFMG C-o.o. phase, all magnetic sites hold roughly the same magnetic moment ( $1.811 \pm 0.002 \mu_B$ ) indicating a purely AFMG magnetic ordering as observed experimentally. Going to the  $P2_1/b$  AFMC G-o.o. phase of  $LaVO_3$ , two magnetic sublattices are observed. Indeed, two different magnitudes for the magnetic moments are found in consecutive  $(xy)$ - $VO_2$  layers ( $1.822 \pm 0.002 \mu_B$  and  $1.813 \pm 0.001 \mu_B$ ) which can be seen as a dominant AFMC ordering plus a smaller AFMG ordering on the top of the latter one.

## **$(AVO_3)_1/(A'VO_3)_1$ layered structures**

Ferroelectric materials possess a spontaneous polarization which is switchable with an electric field. This electric field controlled multi-state system has been naturally proposed as an alternative field effect memory device in electronics.<sup>53</sup> Furthermore, opportunities offered by magneto-electric multiferroics (electric field control of magnetism and conversely) would allow for lower energy consumption spintronic devices.<sup>9,12</sup> However, materials combining both ferroelectric and

(anti)-ferromagnetic order parameters are elusive in nature and the identification of new single phase multiferroics remains a challenge for modern day research.<sup>54,55</sup>

In this respect, a common approach to design multiferroics is to engineer ferroelectricity in magnets.<sup>55</sup> A standard concept to achieve this is *via* the so-called improper ferroelectricity.<sup>56</sup> Here the polarization is not the primary order parameter, as in conventional ferroelectrics, but is driven by one or more primary non-polar modes. A specific emphasis has been dedicated to the rotationally driven ferroelectricity, where one or more AFD motions induce the polarization.<sup>5</sup> This has enabled ferroelectricity in highly strained BiFeO<sub>3</sub>,<sup>57</sup> in short period ABO<sub>3</sub> superlattices,<sup>5-7,17</sup> in Ruddlesden-Popper systems and even in metal organic frameworks.<sup>16,58</sup>

Following the same spirit, in an attempt to engineer ferroelectricity in vanadates, we consider (AVO<sub>3</sub>)<sub>1</sub>/(A'VO<sub>3</sub>)<sub>1</sub> structures with planes of different A cations layered along the [001] direction. This structure can either appear naturally as in the double perovskites, or through single layer precision epitaxial deposition techniques. The free energy expansion around a  $P_4/mmm$  layered reference structure (equivalent to  $Pm\bar{3}m$  in bulk) then becomes:

$$\begin{aligned} \mathcal{F}_{tri,Pb} \propto & \phi_{xy}^- \phi_z^+ P_{xy} + \phi_{xy}^- P_{xy} M_{JT} \\ & + M_{JT} R_{JT} P_z + \phi_z^+ P_z \phi_z^- \end{aligned} \quad (3)$$

The first observation is that the symmetry breaking due to the A cations turns the X antipolar modes to polar modes, i.e. in-plane (110)  $P_{xy}$  and out-of-plane (001)  $P_z$ . The first and fourth trilinear couplings of Equation 3 correspond to the rotationally driven hybrid improper ferroelectricity mechanism.<sup>5-7</sup> However, we identify in vanadate superlattices two new trilinear couplings involving JT distortions (second and third term of Equation 3). We especially highlight the third term of Equation 3,  $M_{JT} R_{JT} P_z$ , which directly couples the out-of-plane polarization  $P_z$  to both JT distortions. Since JT distortions are intimately connected to orbital-orderings and particular magnetic states as described in the previous section, we can expect to have a direct and strong coupling between polarization and magnetism from this term.

In the present work, we have performed first-principles calculations in order to show that  $(\text{AVO}_3)_1/(\text{A}'\text{VO}_3)_1$  layered structures indeed develop both in plane and out-of-plane polarizations.  $P_{xy}$  appears as a slave of rotations and is indirectly linked to magnetism through the modification of the superexchange path as in the usual rotationally driven ferroelectrics.<sup>16</sup> On the other hand,  $P_z$  appears thanks to an electronic instability manifested as a particular orbital and magnetic ordering. Finally, we demonstrate that an electric control of the magnetic state, is indeed possible, providing a novel paradigm for the elusive magnetoelectric multiferroics.

In order to test the above hypothesis, we considered two different superlattices:  $(\text{PrVO}_3)_1/(\text{LaVO}_3)_1$  (PLVO) and  $(\text{YVO}_3)_1/(\text{LaVO}_3)_1$  (YLVO). First principles geometry relaxations (see method section) of the superlattices converged to two metastable states. As in the bulk vanadates, a C-type AFM ordering is found in a  $Pb$  structure (equivalent to the  $P2_1/b$  in bulk) while a G-type AFM ordering is found in a  $Pb2_1m$  symmetry (equivalent to  $Pbnm$  in bulk). We find that PLVO adopts a  $Pb$  AFMC ground state while YLVO adopts a  $Pb2_1m$  AFMG ground state. The symmetry adapted modes and computed polarizations of all metastable phases are presented in the supplementary material. As predicted, the  $Pb2_1m$  ground state of YLVO only exhibits a  $P_{xy}$  polarization of  $7.89 \mu\text{C.cm}^{-2}$ . However, the  $Pb$  ground state of PLVO develops both  $P_{xy}$  and  $P_z$  polarizations of  $2.94$  and  $0.34 \mu\text{C.cm}^{-2}$  respectively. The  $P_z$  contribution indicates, as predicted from the third term of Equation 3, a Jahn-Teller induced ferroelectricity. Below we explore the origin of  $P_{xy}$  and  $P_z$  in more detail.

As we discussed in the first section, bulk vanadates exhibit a  $Pbnm$  phase at room temperature and hence both superlattices should first go to the equivalent  $Pb2_1m$  intermediate phase. We therefore begin by providing insight on the driving force yielding the various distortions within this phase. For this purpose, we condense different amplitudes  $Q$  of distortions (see methods) within the metastable  $Pb2_1m$  state of the PLVO superlattice starting from an ideal  $P_4/mmm$  structure (for each potential, see supplementary material). Four main distortions are then present in this  $Pb2_1m$  phase:  $\phi_{xy}^-$ ,  $\phi_z^+$ ,  $M_{JT}$  and  $P_{xy}$ . As expected, the two AFD motions are strongly unstable (approximately 1 eV of energy gains for each) and are the primary order parameters of this  $Pb2_1m$  symmetry.  $P_{xy}$

and  $M_{JT}$  present single wells which are the signature of an improper anharmonic appearance.<sup>59</sup> Therefore, the  $P_{xy}$  polarization appears through a hybrid improper mechanism driven by the two rotations through the first term of Equation 3. Furthermore, as predicted in the first section, this analysis suggests that the  $M_{JT}$  appears with a structural hybrid improper mechanism rather than an electronic instability.

Having considered the intermediate  $Pb2_1m$  phase, we next turn our attention to the phase transition of PLVO to its  $Pb$  ground state. Curiously, a phonon calculation on the intermediate  $Pb2_1m$  phase did not identify any unstable modes, indicating that no lattice motions can be responsible for the phase transition. Clearly, the system has to switch from G to C-type AFM and therefore in an attempt to understand this phase transition we performed two sets of calculations. The atomic positions were fixed to the intermediate  $Pb2_1m$  structure and the energy was computed i) with imposed and ii) with no imposed,  $Pb2_1m$  symmetry for the electronic wavefunction, both within the two possible magnetic states. While for the AFMG calculations, no energy difference is observed between calculations with and without symmetry, the AFMC calculation with no symmetry leads to a lower energy (around 4.5 meV) than the one with imposed symmetry. The only difference between the two calculations is that the electronic structure is allowed to distort and consequently break the symmetry. We discover that, even with the atoms fixed in centrosymmetric positions (along the  $z$  axis), the electronic instability creates an out-of-plane polarization  $P_z$  of  $0.04 \mu\text{C}\cdot\text{cm}^{-2}$ .

In order to understand the nature of this electronic instability, we plot the projected density of states on vanadiums in 3. Starting from the projected density of states with  $Pb2_1m$  symmetry, consecutive atoms along the  $z$  direction ( $V_1$  and  $V_3$ ,  $V_2$  and  $V_4$  on 2) exhibit identical density of states. Consequently, the orbital ordering appears to be of C-type. When allowing the electronic structure to distort, several changes appear in the orbital occupations. Consecutive atoms along the  $z$  direction now prefer to occupy either more of the  $d_{xz}$  or the  $d_{yz}$  orbital, which results in a mixed G-type plus C-type orbital ordering. The G-o.o. that appears, despite the absence of the  $R_{JT}$  motion, is allowed *via* the Kugel-Khomskii mechanism.<sup>60</sup> This mixed orbital ordering produces an asymmetry between the  $\text{VO}_2$  planes, as indicated by the two magnitudes of magnetic moments

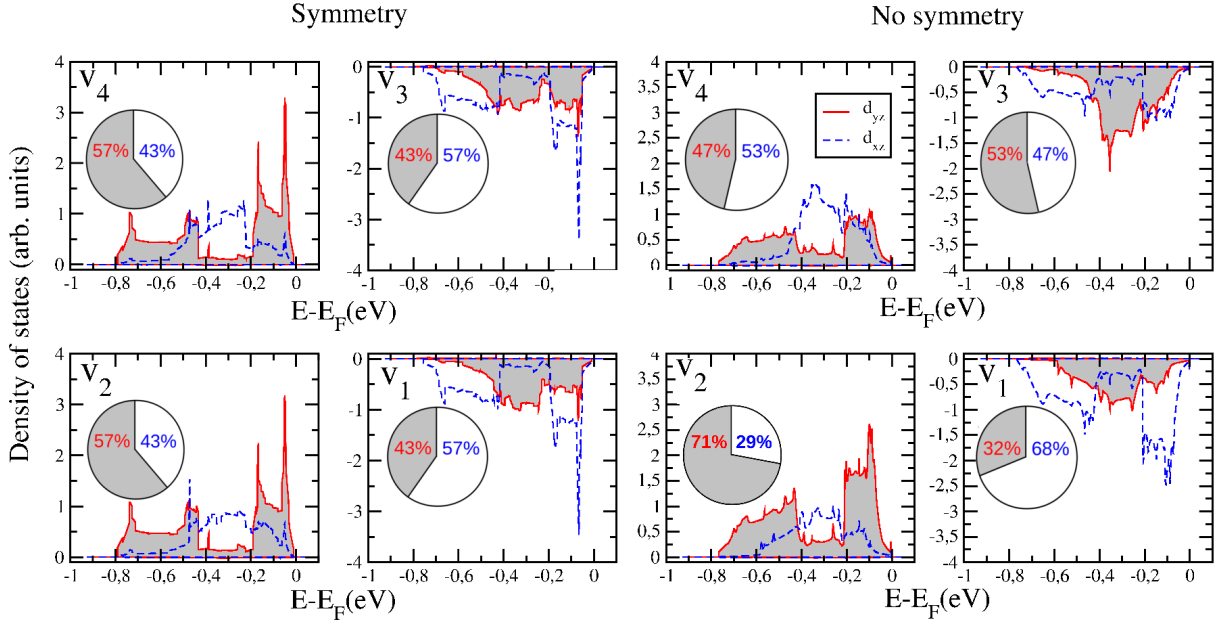


Figure 3: Projected density of states on the  $d_{yz}$  (grey filled red curve) and  $d_{xz}$  (unfilled blue dashed curve) orbitals of vanadium by imposing the  $Pb2_1m$  atomic positions and computing the energy with  $Pb2_1m$  symmetry (left) for the electronic wavefunction and by removing the symmetry (right) for the electronic wavefunction.  $d_{xy}$  is not displayed for clarity.  $V_1$  ( $V_3$ ) and  $V_2$  ( $V_4$ ) are located within the same (001) plane as defined in 2. The percentage of total  $d_{yz}$  (red) and  $d_{xz}$  (blue) character on each vanadium is shown as a pie chart to illustrate the change from C-o.o to C+G-o.o. once the symmetry constraint for the wavefunction is lifted.

in each layer ( $1.816 \pm 0.001 \mu_B$  and  $1.819 \pm 0.001 \mu_B$ ). The mixed orbital ordering also appears in the bulk vanadates, such as the G-o.o.+C-o.o. ground state of  $\text{LaVO}_3$  (previously thought to be just G-o.o. from experiments).<sup>4,25</sup> However, here it is not enough to break the inversion symmetry along the  $z$  axis yielding no out-of-plane polarization. The second necessary ingredient is the symmetry breaking due to the A and A' ordering along the [001] direction in the superlattices. The combination of both effects (in the AO and  $\text{VO}_2$  planes) is required to break inversion symmetry along the  $z$  axis and to produce the out-of-plane polarization. The result is an orbital ordering induced ferroelectricity in vanadate superlattices.

Interestingly, the direction of the orbital ordering induced ferroelectric polarization is found to be arbitrary, and both  $+0.04$  and  $-0.04 \mu\text{C}\cdot\text{cm}^{-2}$  are observed. Each state displays a reversal of the magnitude of the magnetic moment of the two  $\text{VO}_2$  planes. Starting from these two possibilities, we performed the geometry relaxation and it ended with the previously identified  $Pb$  ground states, with both possibilities (up and down) for the out-of-plane polarization. We note that the difference in magnetic moment between both  $\text{VO}_2$  planes is more pronounced ( $1.820 \pm 0.001 \mu_B$  and  $1.828 \pm 0.001 \mu_B$ ) after the geometry relaxation. Three new lattice distortions develop to reach the  $Pb$  phase:  $P_z$ ,  $R_{JT}$  and  $\phi_z^-$ . To understand the nature of their appearance, we plot in 4 each potential as a function of its amplitude  $Q$ . All potentials present single wells, more or less shifted through an improper coupling with the electronic instability. This confirms that the electronic instability is the primary order parameter driving the phase transition. Moreover, the  $R_{JT}$  motion presents an energy gain of one to two orders of magnitude larger than those of the  $\phi_z^-$  motion, indicating that the  $R_{JT}$  couples more strongly with the electronic instability, which might be expected. Consequently, once the electronic instability condenses, the  $R_{JT}$  lattice distortion is forced into the system and finally, this latter produces the lattice part of the polarization through the structural hybrid improper coupling. This Jahn-Teller induced ferroelectricity amplifies by one order of magnitude the electronic out-of-plane polarization. The sign of the three lattice distortions is again imposed by the initial sign (up or down) of the electronic polarization. Consequently, the reversal of  $P_z$  through an application of an external electric field would require the reversal of both  $R_{JT}$ ,  $\phi_z^-$

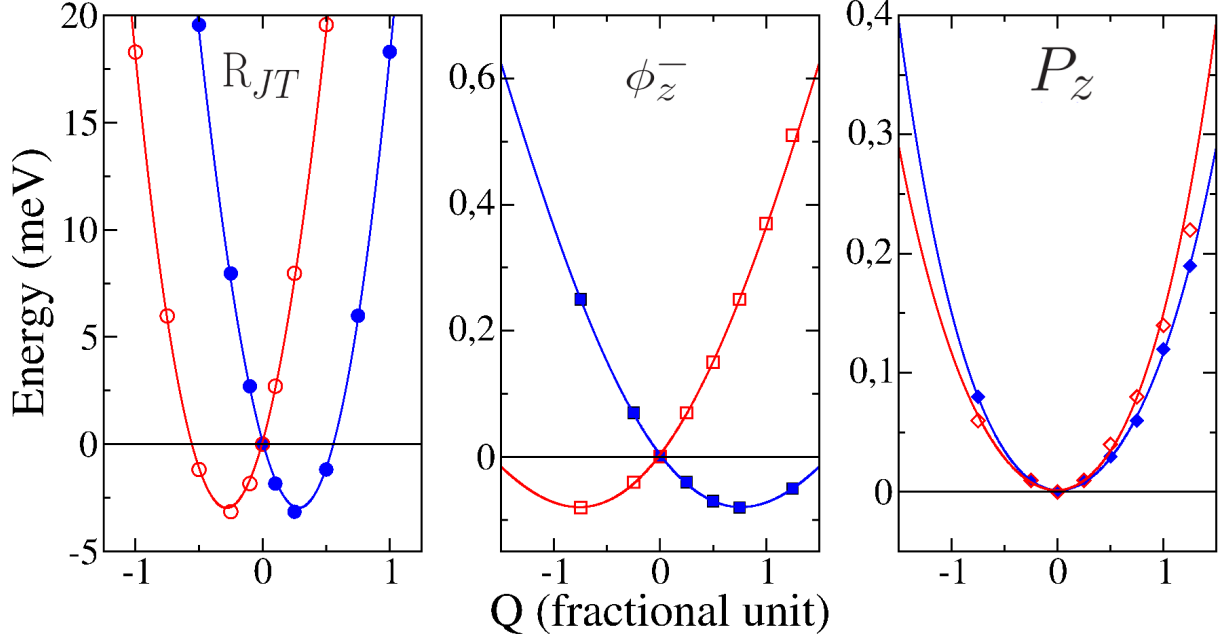


Figure 4: Energy gains (in meV) by condensing various amplitudes of the individual  $R_{JT}$ ,  $\phi_z^-$  and  $P_z$  distortions. Potentials are plotted for a ' $\uparrow$ ' (filled blue symbols) and a ' $\downarrow$ ' (unfilled red symbols) initial electronic polarization.

and the magnitude if the magnetic moment of both  $\text{VO}_2$  planes. The saddle point at the midway of this reversal (all three modes equal zero, i.e. the  $Pb2_1m$  phase) is of the order of 10 meV higher in energy, which represents a reasonable estimate of the ferroelectric switching barrier. Compared to the rotationally driven ferroelectricity  $P_{xy}$ , whose energy barrier is of the order of 0.1 to 1 eV,<sup>6,17,18</sup> this Jahn-Teller induced ferroelectricity is therefore very likely to be switchable. The large difference between the two energy barriers is due to two different energy landscapes involving i) the robust AFD motions inducing  $P_{xy}$  and ii) the relatively soft distortions inducing  $P_z$ .

Finally we discuss a novel route to create the technologically desired electrical control of magnetization. Starting from a  $Pb2_1m$  phase with an AFMG magnetic ordering, the application of an external electric field  $\vec{E}$  along  $z$  will induce  $P_z$  in the system through the dielectric effect. As a result, the  $R_{JT}$  distortion is automatically induced through the  $M_{JT}R_{JT}P_z$  trilinear term. This electric field induced  $R_{JT}$  distortion is a general result for any  $(ABO_3)_1/(A'BO_3)_1$  superlattice consisting of two  $Pbnm$  perovskites. Since  $R_{JT}$  distortions are intimately connected to the G-o.o. and the AFMC

magnetic ordering, for a finite value of  $\vec{E}$ , the system may switch from the initial AFMG phase to the AFMC phase. In reality, the AFMC phase should exhibit a net weak magnetization from a non collinear magnetic structure as observed in several bulk vanadates of  $P2_1/b$  symmetry.<sup>28,30</sup> Therefore, the application of an electric field may not only switch between AFM orderings, but also produce a net magnetic moment in the material. However, even at the collinear level in our calculations, we can look at the relative stability between the two magnetic states under an external electric field in the YLVO superlattice, which presents the desired  $Pb2_1m$  ground state (8 meV lower than the  $Pb$  phase).

5 (top panel) plots the free electric energy (see methods) between the two phases as a function of an electric field applied along the  $z$  direction. As the electric field increases in the system, the

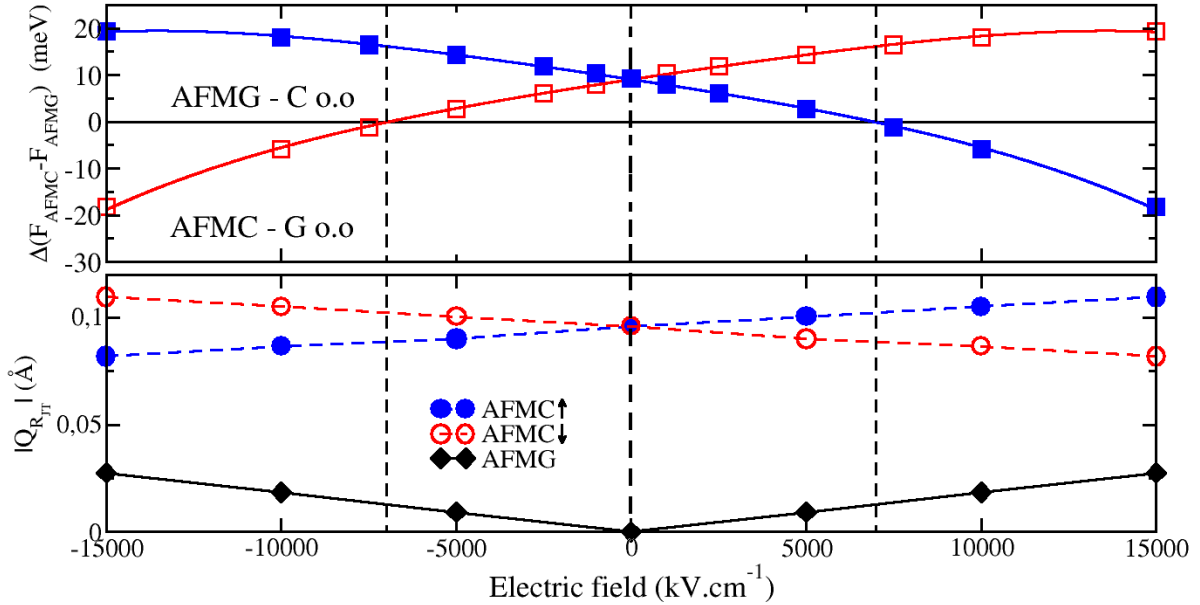


Figure 5: (top) Free electric energy difference (in meV) between the two different phases of YLVO superlattices under an applied electric field along the  $z$  direction. The red unfilled (blue filled) symbols correspond to a configuration starting with an  $\downarrow$  ( $\uparrow$ ) electronic polarization. (bottom) Amplitude of  $R_{JT}$  distortion as a function of the electric field applied along the  $z$  direction in the  $Pb2_1m$ -AFMG phase (filled diamonds) and in the  $Pb$ -AFMC phase (circles).

relative free energy difference between the two phases reduces, and indeed at around  $7 \text{ MV}\cdot\text{cm}^{-1}$ , the  $Pb$ -AFMC phase becomes more stable than the initial  $Pb2_1m$ -AFMG phase. This electric field value corresponds to a voltage of 0.55 V for one bilayer ( $c \simeq 7.8 \text{ \AA}$ ). The critical electric field can



be minimized by reducing the energy difference between the two phases at zero field. This can be achieved by for example changing the rare earth cations or applying biaxial epitaxial strain (see supplementary material).

More generally, we demonstrate in the present study an electric field control of the Jahn-Teller distortions (see 5 bottom). Since this mechanism arises from universal symmetry relations, we can expect this effect to also appear in other perovskite superlattices. This effect may find applications outside the field of magnetoelectrics such as for tunable band gaps and metal-insulator transitions, since the Jahn-Teller distortion affects the electronic structure in general.

## Conclusions

In conclusion, we have identified novel lattice mode couplings in the vanadates, helping to clarify the origin of the unusual coexisting Jahn-Teller phase, and indeed the role of Jahn-Teller distortions in perovskites in general. These findings have enabled the prediction of a novel paradigm for the elusive magnetoelectric multiferroics, based on a Jahn-Teller / orbital ordering induced ferroelectricity. Due to the intimate connection between Jahn-Tellers and orbital ordering with magnetism, this unprecedented type of improper ferroelectric facilitates an electric field control of magnetization. The rationale is completely general, and a challenge for applications will be to identify new materials with a magnetic and co-existing Jahn-Teller phase at room temperature. The demonstration of an electric field control of Jahn-Teller distortions may find more general applications for novel functional devices, outside the field of multiferroics. We hope these discoveries will help motivate future studies that will further unlock the potential of vanadate perovskites, and other Jahn-Teller systems.

## Methods

The basic mechanism we propose here is solely based on symmetry arguments. Symmetry mode analysis of experimental data were performed using amplimodes.<sup>47,48</sup> The free energy expansion

of Equations 1, 2 and 3 is performed using the invariants software from the isotropy code.<sup>61</sup> The results from these symmetry considerations are not dependent on the technical parameters of the first-principles calculations. The latter are only there to illustrate on a concrete basis and quantify the effect. First principles density functional theory calculations were performed using the VASP package.<sup>62,63</sup> We used a  $6 \times 6 \times 4$  Monkhorst-Pack k-point mesh to model the *Pbnm* ( $P2_1/b$ ) phase and a plane wave cut off of 500 eV.<sup>64</sup> Optimized Projector Augmented wave (PAW) potentials for PBEsol exchange-correlation functional were used in the calculations.<sup>65</sup> The polarization was computed using the Berry phase approach as implemented in VASP.<sup>66,67</sup> The study was performed within the LDA+U framework using an effective  $U_{\text{eff}}$ .<sup>68-70</sup> The LDA+U framework has already been shown to be sufficient to reproduce the ground state of vanadates.<sup>39,71</sup> The effective  $U_{\text{eff}}$  parameter was first fitted on bulk compounds in order to correctly reproduce the ground state of the bulk vanadates. A value of  $U_{\text{eff}}=3.5$  eV was obtained (see Table 2 and Table 3 in the supplementary material). Phonon calculations were performed using the density functional perturbation theory.<sup>72</sup> We utilized a collinear approach to model the magnetic structures. Structural relaxations were performed until the maximum forces were below  $5 \mu\text{eV}\cdot\text{\AA}^{-1}$  and the energy difference between conjugate gradient steps was less than  $10^{-9}$  eV. The superlattices were relaxed starting from four different initial guesses: two magnetic orderings (C- and G-type AFM) and two space groups (*Pb2<sub>1</sub>m* and *Pb*, subgroups of *Pbnm* and  $P2_1/b$  respectively for the layered structures). Lattice distortion potentials were plotted as a function of the amplitude  $Q$  of each mode separately.  $Q$  is defined as the fraction of the amplitude of the distortion with respect to the ground state. The electric field effect on the system was modeled using a linear response resulting in an ionic relaxation.<sup>73</sup> Since an electric field is applied on the system, the free energy of the system becomes

$$\mathcal{F} = E_{KS} - \Omega \vec{E} \cdot \vec{P} \quad (4)$$

where  $E_{KS}$  is the Kohn-Sham energy,  $\Omega$  is the unit cell volume.

## Acknowledgement

Ph. Ghosez acknowledges Research Professorship from the Francqui foundation and the ARC project TheMoTherm. Calculations have been performed within the PRACE projects TheoMoMu-LaM and TheDeNoMo and on Nic4 cluster at ULg. Authors acknowledge fruitful discussions with D. Fontaine, J. M. Triscone and M. Verstraete.

## References

- (1) J. G. Bednorz, K. A. Müller, *Physik B Cond. Matter* **1986**, *64*, 189.
- (2) M. Wu, J. Ashburn, C. Torng, P. H. Hor, R. Meng, L. Gao, Z. Huang, Y. Wang, C. Chu, **1987**, *58*, 908.
- (3) G. Jonker, J. Van Santen, *Physica* **1950**, *16*, 337.
- (4) S. Jin, T. H. Tiefel, M. McCormack, R. Fastnacht, R. Ramesh, L. Chen, *Science* **1994**; *264*, 413.
- (5) P. Zubko, S. Gariglio, M. Gabay, P. Ghosez, J.-M. Triscone, *Annu. Rev. Condens. Matter Phys.* **2011**, *2*, 141.
- (6) H. Hwang, Y. Iwasa, M. Kawasaki, B. Keimer, N. Nagaosa, Y. Tokura, *Nature Materials* **2012**, *11*, 103.
- (7) Y. Tokura, N. Nagaosa, *Science* **2000**, *288*, 462.
- (8) E. Dagotto, *Science* **2005**, *309*, 257.
- (9) M. Bibes, A. Barthélémy, *Nature Materials* **2008**, *7*, 425.
- (10) J. Mannhart, D. Schlom, *Science* **2010**, *327*, 1607.
- (11) J. Scott, *Science* **2007**, *315*, 954.

- (12) J. Scott, *Nature Materials* **2007**, *6*, 256.
- (13) E. Bousquet, M. Dawber, N. Stucki, C. Lechtensteiger, P. Hermet, S. Gariglio, J. M. Gariglio, P. Ghosez, *Nature* **2008**, *452*, 732.
- (14) T. Fukushima, A. Stroppa, S. Picozzi, J. M. Perez-Mato, *Phys. Chem. Chem. Phys.* **2011** , *13*, 12186.
- (15) J. M. Rondinelli, C. J. Fennie, *Adv. Materials* **2012**, *24*, 1961.
- (16) N. A. Benedek, C. J. Fennie, *Phys. Rev. Lett.* **2011**, *106*, 107204.
- (17) Z. Zanolli, J. C. Wojdel, J. Iñiguez, P. Ghosez, *Phys. Rev. B* **2013**, *88*, 060102(R).
- (18) A. T. Mulder, N. A. Benedek, J. M. Rondinelli, C. J. Fennie, *Adv. Func. Mater.* **2013**, *23*, 4810.
- (19) H. Köppel, D. R. Yarkony, H. Barentzen, *The Jahn-Teller Effect*, Springer, 2009.
- (20) M. Onoda, H. Ohta, H. Nagasawa, *Solid State Comm.* **1991**, *79*, 281.
- (21) A. Wold, R. Ward, *J. Am. Chem. Soc.* **1954**, *76*, 1029.
- (22) G. Bowden, *Australian Journal of Physics* **1998**, *51*, 201.
- (23) P. Bordet, C. Chailout, M. Marezio, Q. Huang, A. Santoro, S. Cheong, H. Takagi, C. Oglesby, B. Batlogg, *J. Solid State Chem.* **1993**, *106*, 253.
- (24) H. Kawano, H. Yoshizawa, Y. Ueda, *J. Phys. Soc. Jpn* **1994**, *63*, 2857.
- (25) S. Miyasaka, Y. Okimoto, M. Iwama, Y. Tokura, *Phys. Rev. B* **2003**, *68* , 100406.
- (26) M. Sage, G. Blake, C. Marquina, T. Palstra, *Phys. Rev. B* **2007**, *76*, 195102.
- (27) A. Mahajan, D. Johnston, D. Torgeson, F. Borsa, *Phys. Rev. B* **1992**, *46*, 10966.

- (28) Y. Ren, T. Palstra, D. Khomskii, E. Pellegrin, A. Nugroho, A. Menovsky, G. Sawatzky, *Nature* **1998**, *396*, 441.
- (29) L. Tung, A. Ivanov, J. Schefer, M. R. Lees, G. Balakrishnan, D. M. Paul, *Phys. Rev. B* **2008**, *78*, 054416.
- (30) L. Tung, M. Lees, G. Balakrishnan, D. M. Paul, *Phys. Rev. B* **2007**, *75*, 104404.
- (31) H. Nakotte, L. Laughlin, H. Kawanaka, D. Argyriou, R. Sheldon, Y. Nishihara, *J. App. Phys.* **8** **1999**, *5*, 4850.
- (32) C. Ulrich, G. Khaliullin, J. Sirker, M. Reehuis, M. Ohl, S. Miyasaka, Y. Tokura, B. Keimer, *Phys. Rev. Lett.* **2003**, *91*, 257202.
- (33) A. Tsvetkov, F. Mena, P. Van Loosdrecht, D. Van Der Marel, Y. Ren, A. Nugroho, A. Menovsky, I. Elfimov, G. Sawatzky, *Phys. Rev. B* **2004**, *69*, 075110.
- (34) T.-h. Arima, Y. Tokura, *J. Phys. Soc. Jpn* **1995**, *64*, 2488.
- (35) M. Noguchi, A. Nakazawa, S. Oka, T. Arima, Y. Wakabayashi, H. Nakao, Y. Murakami, *Phys. Rev. B* **2000**, *62*, 9271(R).
- (36) G. Khaliullin, P. Horsch, A. M. Oleś, *Phys. Rev. Lett.* **2001**, *86*, 3879.
- (37) H. Sawada, K. Terakura, *Phys. Rev. B* **1998**, *58*, 6831.
- (38) G. R. Blake, T. Palstra, Y. Ren, A. A. Nugroho, A. Menovsky, *Phys. Rev. Lett.* **2001**, *87*, 245501.
- (39) M. De Raychaudhury, E. Pavarini, O. Andersen, *Phys. Rev. Lett.* **2007**, *99*, 126402.
- (40) H. A. Jahn, E. Teller, *Proc. Royal Soc. London Series A - Mathematical and Physical Sciences* **1937**, *161*, 220.

- (41) We note here the distinction between the Jahn-Teller effect and what we call the Jahn-Teller distortion in this study. Here we define the Jahn-Teller distortion by the symmetry of the atomic distortion as shown in Figure 1.b and Figure 1.d. Whilst a distortion of this symmetry will by definition remove the *d* electronic degeneracy, the origin of such a distortion does not necessarily need to appear from the Jahn-Teller effect. An important result of this study is that the Jahn-Teller distortion can instead appear through structural anharmonic couplings.
- (42) H. Kramers, *Physica* **1934**, *1*, 182.
- (43) P. Anderson, *Phys. Rev.* **1950**, *79*, 350.
- (44) J. B. Goodenough, *Phys. Rev.* **1955**, *100*, 564.
- (45) J. B. Goodenough, *J. Phys. Chem. Solids* **1958**, *6*, 287.
- (46) J. Kanamori, *J. Phys. Chem. Solids* **1959**, *10*, 87.
- (47) D. Orobengoa, C. Capillas, M. I. Aroyo, J. M. Perez-Mato, *J. App. Cryst.* **2009**, *42*, 820.
- (48) J. Perez-Mato, D. Orobengoa, M. Aroyo, *Acta Cryst. A* **2010**, *66*, 558.
- (49) M. Reehuis, C. Ulrich, P. Pattison, B. Ouladdiaf, M. Rheinstädter, M. Ohl, L. Regnault, M. Miyasaka, Y. Tokura, B. Keimer, *Phys. Rev. B* **2006**, *73*, 094440.
- (50) H. Seim, H. Fjellvag, , *Acta Chem. Scand.* **1998**, *52*, 1096.
- (51) A. Glazer, *Acta Cryst. B* **1972**, *28*, 3384.
- (52) V. M. Goldschmidt, *Naturwissenschaften* **1926**, *14*, 477.
- (53) J. F. Scott, C. A. P. De Araujo, *Science* **1989**, *246*, 1400.
- (54) N. A. Hill, *J. Phys. Chem. B* **2000**, *104*, 6694.
- (55) J. Varignon, N. C. Bristowe, E. Bousquet, P. Ghosez, *Compte Rendu de l'Académie des Sciences*, *in preparation*.

- (56) A. Levanyuk, D. G. Sannikov, *Physics-Uspekhi* **1974**, *17*, 199.
- (57) Y. Yang, W. Ren, M. Stengel, X. H. Yan, L. Bellaïche, *Phys. Rev. Lett.* **2012**, *109*, 057602.
- (58) A. Stroppa, P. Barone, P. Jain, J. M. Perez-Mato, S. Picozzi, *Adv. Mater.* **2013**, *25*, 2284.
- (59) P. Ghosez, J. M. Triscone, *Nature Materials* **2011**, *10*, 269.
- (60) K. Kugel, D. Khomskii, *Zh. Eksp. Teor. Fiz* **1973**, *64*, 1429.
- (61) D. M. Hatch, H. T. Stokes, *J. App. Cryst.* **2003**, *36*, 951.
- (62) G. Kresse, J. Haffner, *Phys. Rev. B* **1993**, *47*, 558.
- (63) G. Kresse, J. Furthmüller, *Comp. Mat. Science* **1996**, *6*, 15.
- (64) H. J. Monkhorst, J. D. Pack, *Phys. Rev. B* **1976**, *13*, 5188.
- (65) J. P. Perdew, A. Ruzsinszky, G. I. Csonka, O. A. Vydrov, G. E. Scuseria, L. A. Constantin, X. Zhou, K. Burke, *Phys. Rev. Lett.* **2008**, *100*, 136406.
- (66) R. Resta, *Ferroelectrics* **1992**, *136*, 51.
- (67) R. D. King-Smith, D. Vanderbilt, *Phys. Rev. B* **1993**, *47*, 1651.
- (68) V. I. Anisimov, J. Zaanen, O. K. Andersen, *Phys. Rev. B* **1991**, *44*, 943.
- (69) A. I. Liechtenstein, V. I. Anisimov, J. Zaanen, *Phys. Rev. B* **1995**, *52*, 5467(R).
- (70) S. L. Dudarev, G. A. Botton, S. Y. Savrasov, C. J. Humphreys, A. P. Sutton, *Phys. Rev. B* **1998**, *57*, 1505.
- (71) Z. Fang, N. Nagaosa, *Phys. Rev. Lett.* **2004**, *93*, 176404.
- (72) S. Baroni, S. de Gironcoli, A. Dal Corso, P. Giannozzi, *Rev. Mod. Phys.* **2001**, *73*, 515.
- (73) X. Gonze, C. Lee, *Phys. Rev. B* **1997**, *55*, 10355.

# Supplementary Material

## Optimized bulk vanadates at 0K

In order to extract the effective  $U_{\text{eff}}$  parameter for our DFT calculations, we fitted its value on bulk vanadates in order to correctly reproduce the ground state of  $\text{YVO}_3$ ,  $\text{PrVO}_3$  and  $\text{LaVO}_3$ . With an effective parameter of  $U_{\text{eff}}$  of 3.5 eV, we correctly reproduce the  $Pbnm$  ground state of  $\text{YVO}_3$  and the  $P2_1/b$  ground state of both  $\text{PrVO}_3$  and  $\text{LaVO}_3$ . Optimized lattice parameters and symmetry mode analysis are given in 2 and 3 respectively. Within our DFT calculations,  $\text{YVO}_3$  exhibits a gap of 1.95 eV in close comparison with experimental value (around 1.6 eV),<sup>1</sup> while  $\text{LaVO}_3$  and  $\text{PrVO}_3$  develop band gaps of 1.70 eV and 1.93 eV respectively.

Table 2: Optimized lattice parameters for the bulk vanadates at 0 K. Experimental values are given for comparison.

		$\text{YVO}_3$		$\text{PrVO}_3$	$\text{LaVO}_3$
		$Pbnm$	$P2_1/b$	$P2_1/b$	$P2_1/b$
		AFMG	AFMC	AFMC	AFMC
a(Å)	th.	5.28	5.27	5.48	5.55
	exp.	5.29(5K) <sup>2</sup>	5.28(85K) <sup>2</sup>	5.48(5K) <sup>4</sup>	5.56(10K) <sup>23</sup>
b (Å)	th.	5.61	5.65	5.68	5.64
	exp.	5.59(5K) <sup>2</sup>	5.62(85K) <sup>2</sup>	5.61(5K) <sup>4</sup>	5.59(10K) <sup>23</sup>
c (Å)	th.	7.58	7.55	7.72	7.76
	exp.	7.56(5K) <sup>2</sup>	7.54(85K) <sup>2</sup>	7.69(5K) <sup>4</sup>	7.75(10K) <sup>23</sup>
$\alpha$ (°)	th.	-	90.03	90.14	90.15
	exp.	-	90.02(85K) <sup>2</sup>	90.15(5K) <sup>4</sup>	90.13(10K) <sup>23</sup>

## Optimized $(\text{AVO}_3)_1/(\text{A}'\text{VO}_3)_1$ layered structures

### Symmetry mode analysis

Symmetry mode analysis of our optimized vanadate layered structures are provided in 4. The superlattice is insulating and develops a band gap of 1.86 eV.



Table 3: Amplitudes of distortions (in Å) on our optimized bulk vanadates at 0 K with respect to a hypothetical pseudocubic phase. In the  $P2_1/b$  symmetry, both  $\phi_{xy}^-$  and  $\phi_z^-$  belong to the same irreps, even if  $\phi_z^-$  amplitude of distortion should remain extremely small.

	YVO <sub>3</sub>		PrVO <sub>3</sub>	LaVO <sub>3</sub>
	<i>Pbnm</i>	<i>P2<sub>1</sub>/b</i>	<i>P2<sub>1</sub>/b</i>	<i>P2<sub>1</sub>/b</i>
$\phi_{xy}^- (+ \phi_z^-)$	-	1.81	1.42	1.32
$\phi_{xy}^-$	1.83	-	-	-
$\phi_z^+$	1.24	1.25	0.97	0.89
$M_{JT}$	0.15	0.06	0.02	0.01
$R_{JT}$	-	0.10	0.10	0.09
$X_5^-$	0.90	0.90	0.65	0.52
$X_3^-$	-	0.05	0.01	0.00

Table 4: Symmetry allowed distortions (in Å) with respect to a hypothetical  $P_4/mmm$  phase of the ground states of the different superlattices. A full relaxation of the reference  $P_4/mmm$  structures was performed before the symmetry mode analysis. Within the  $Pb$  symmetry,  $\phi_{xy}^-$  and  $\phi_z^-$  do not belong to the same irreps any more, clearly showing a non-zero  $\phi_z^-$  contribution, confirming the  $a^-a^-c^\pm$  tilt system.

	YLVO (0K)	PLVO (0K)
	<i>Pb2<sub>1</sub>m-AFMG</i>	<i>Pb-AFMC</i>
$\phi_{xy}^-$	1.58	1.36
$\phi_z^+$	1.13	0.94
$\phi_z^-$	-	0.01
$M_{JT}$	0.13	0.01
$R_{JT}$	-	0.09
$P_{xy}$	0.76 (7.89 $\mu C.cm^{-2}$ )	0.59 (2.94 $\mu C.cm^{-2}$ )
$P_z$	-	0.00(4) (0.34 $\mu C.cm^{-2}$ )

## Origin of $P_{xy}$

As discussed in the main paper, bulk vanadates develop a  $Pbnm$  symmetry at room temperature and hence the layered structures should present the equivalent  $Pb2_1m$  symmetry. In the  $Pb2_1m$  phase, four main distortions are present:  $\phi_{xy}^-$ ,  $\phi_z^+$ ,  $M_{JT}$  and  $P_{xy}$ . In order to understand the driving force leading to this metastable  $Pb2_1m$  symmetry, we added some amplitude  $Q$  of distortions leading to this symmetry in a hypothetical  $P4/mmm$  phase. Potentials are plotted in figure 6. As expected,

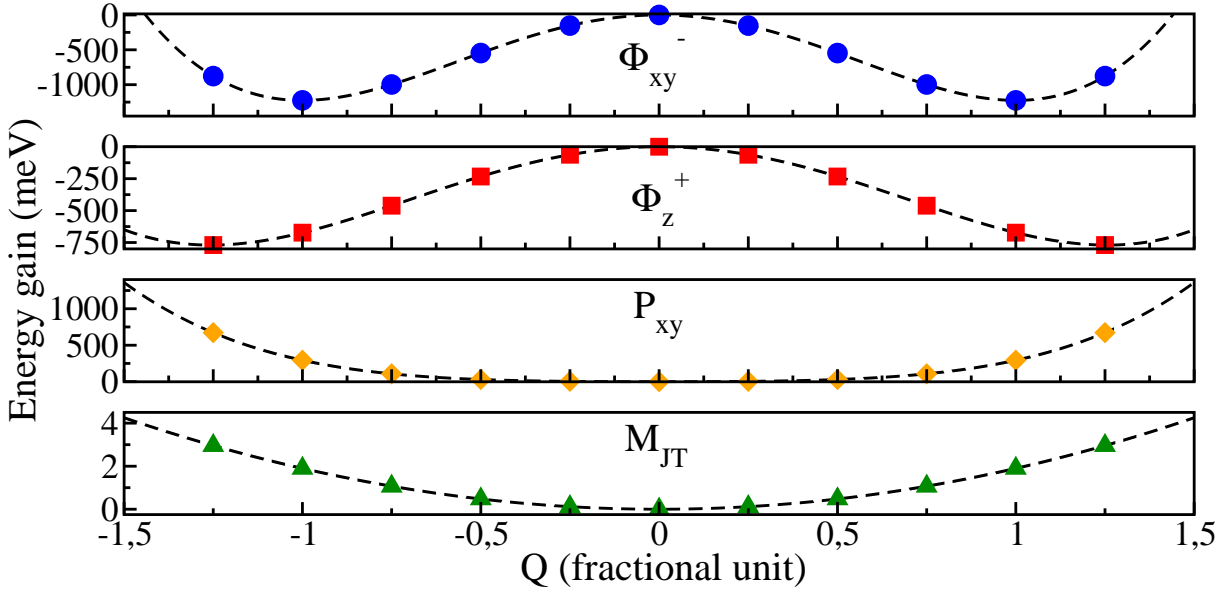


Figure 6: Energy gains (in meV) by condensing several amplitudes of distortions leading to the  $Pb2_1m$  (AFMG) within the  $P4/mmm$  structure.

the two AFD motions present double wells and are strongly unstable (energy gains around 1 eV) while  $P_{xy}$  and  $M_{JT}$  are stable. Consequently,  $\phi_{xy}^-$  and  $\phi_z^+$  are the primary order parameters leading to the  $Pb2_1m$  symmetry, and  $P_{xy}$  and  $M_{JT}$  appear through improper couplings. These potentials confirm the hybrid improper character of  $P_{xy}$ .<sup>5-7</sup>

## Strain effect on $(AVO_3)_1/(A'VO_3)_1$ layered structures

For potential applications, the proposed superlattices can be grown on given substrates. The pseudocubic parameters (defined as the mean value of the low symmetry lattice parameters) are 3.88 Å, 3.88 Å and 3.92 Å for YLVO and PLVO superlattices respectively. We chose cubic SrTiO<sub>3</sub> (3.905 Å)

and  $\text{KTaO}_3$  (3.9885 Å) as two potential substrates and performed a geometry relaxation of the two superlattices constraining both in-plane pseudocubic lattice parameters to those of the substrates.<sup>8</sup> Results are displayed in 5. The effect of the substrates is to tune the relative energy difference

Table 5: Energy differences  $\Delta E$  (in meV) between the two magnetic states with respect to the AFMG structure on the two different substrates. The fully relaxed energy difference is given for comparison.

		SrTiO <sub>3</sub>		Fully relaxed		KTaO <sub>3</sub>	
		AFMG	AFMC	AFMG	AFMC	AFMG	AFMC
YLVO	$\Delta E$	0	+24	0	+8	0	-10
	$c/a$	0.98	0.98	1.01	1.01	0.95	0.95
PLVO	$\Delta E$	0	+8	0	-4	0	-13
	$c/a$	1.00	1.00	1.00	1.00	0.96	0.96

between the two magnetic orderings, and hence between the two orbital-ordered phases. A SrTiO<sub>3</sub> substrate seems to favor an AFMG magnetic ordering, and consequently a pure  $M_{JT}$  phase. On the contrary, going to a KTaO<sub>3</sub> substrate applies a moderate tensile strain and favors an AFMC magnetic ordering for the two superlattices. These strain effects then open the way to an indirect control of the magnetism and the orbital ordering playing with the strain imposed by the substrates. Indeed, growing  $(\text{AVO}_3)_1/(\text{A}'\text{VO}_3)_1$  layered structures on a piezoelectric substrates, an indirect coupling with the electric field may appear:

$$\text{coupling} \propto \frac{\text{electric}}{\text{strain}} \times \frac{\text{strain}}{\text{magnetism}}$$

Applying an external field on the substrate induces a strain on the vanadate layered structure, and consequently this latter can switch both magnetic and orbital orderings.

## References

- (1) A. Tsvetkov, F. Mena, P. Van Loosdrecht, D. Van Der Marel, Y. Ren, A. Nugroho, A. Menovsky, I. Elfimov, G. Sawatzky, Phys. Rev. B **2004**, 69, 075110.

- (2) M. Reehuis, C. Ulrich, P. Pattison, B. Ouladdiaf, M. Rheinstädter, M. Ohl, L. Regnault, M. Miyasaka, Y. Tokura, B. Keimer, *Phys. Rev. B* **2006**, *73*, 094440.
- (3) M. Sage, G. Blake, C. Marquina, T. Palstra, *Phys. Rev. B* **2007**, *76*, 195102.
- (4) M. Sage, G. Blake, C. Marquina, T. Palstra, *Phys. Rev. B* **2007**, *76*, 195102.
- (5) E. Bousquet, M. Dawber, N. Stucki, C. Lechtensteiger, P. Hermet, S. Gariglio, J. M. Gariglio, Ph. Ghosez, *Nature* **2008**, *452*, 732.
- (6) J. M. Rondinelli, C. J. Fennie, *Adv. Materials* **2012**, *24*, 1961.
- (7) T. Fukushima, A. Stroppa, S. Picozzi, J. M. Perez-Mato, *Phys. Chem. Chem. Phys.* **2011**, *13*, 12186.
- (8) D. G. Schlom, L.-Q. Chen, C.-B. Eom, K. M. Rabe, S. K. Streiffer, J.-M. Triscone, *Annu. Rev. Mater. Res.* **2007**, *37*, 589.